Soft Matter

PAPER

View Article Online
View Journal | View Issue

Cite this: *Soft Matter*, 2016, 12, 8407

Nanoparticle diffusion in crowded and confined media†

Firoozeh Babayekhorasani,[a] Dave E. Dunstan,[b] Ramanan Krishnamoorti*[ac] and Jacinta C. Conrad*[a]

Received 6th July 2016,
Accepted 11th September 2016

DOI: 10.1039/c6sm01543c

www.rsc.org/softmatter

We identify distinct mechanisms controlling slowing of nanoparticle diffusion through complex media featuring both rigid geometrical confinement and soft mobile crowders. Towards this end, we use confocal microscopy and single particle tracking to probe the diffusion of 400 nm nanoparticles suspended in Newtonian water, in a Newtonian glycerol/water mixture, or in a non-Newtonian polymer solution through a model porous medium, a packed bed of microscale glass beads. The mobility of nanoparticles, as quantified by the long-time diffusion coefficient extracted from the particle mean-squared displacement, slows as the average pore size of the packed bed media decreases for both Newtonian and non-Newtonian solutions. The distribution of particle displacements is non-Gaussian, consistent with the spatial heterogeneity of the geometrical confinement imposed by the packed bed. The slowing of nanoparticle mobility in all solutions follows the predictions of models that describe hydrodynamic interactions with the packed bed. In non-Newtonian solutions, depletion interactions due to the polymers near the glass beads result in temporary adsorption of particles onto the bead surface, as indicated by a stretched-exponential distribution of residence times. Our results therefore suggest that the confined diffusive dynamics of nanoparticles in polymer solutions is controlled by two competing mechanisms: hydrodynamic interactions between particles and spatial obstacles, which dictate the long-time slowing of diffusion, and depletion interactions between particles and confining walls due to the macromolecules, which control transient adsorption and hence alter the statistics of the short-time motion.

Introduction

Confinement by rigid hard obstacles and compliant soft matrices alters the transport of nanoscale particles in complex media. For example, within biological cells nanoscale cargos diffuse through the crowded cytoplasm and through a network of rigid microtubules and/or semiflexible actin filaments.[1–6] Similarly, delivering drugs, diagnostics, or therapeutic agents to targeted tissues in the human body requires transport through the rigid extracellular matrix and the extracellular fluid volume,[7–9] or through the highly selective blood–brain barrier.[10] Separations in size-exclusion chromatography[11] and in membranes[12] rely on rigid structures to separate nanoscale particles from concentrated soft-matter solutions containing polymers, surfactants, proteins, or micelles. Finally, effectively dispersing engineered nanomaterials in fiber-reinforced composites during processing involves transport through a polymer solution or melt as well as through the rigid fiber network.[13–15] In each of these settings, nanoparticle diffusion is hindered by confinement and by crowding; in turn, slowed diffusion can reduce, as one example, the rate at which reactions occur.[16] Understanding the competing effects of crowding *versus* confinement on diffusive slowing is therefore expected to give insight into a wide range of biological, chemical, and physical processes that involve hindered transport.

In a rigid porous medium, nanoparticle mobility is influenced by hydrodynamic and excluded-volume interactions and hence dictated by the geometry of the medium. Spatial structure,[17–20] void accessibility,[21] and connectivity of the porous medium[22] alter, through hydrodynamic and steric interactions, the diffusive mobility of particles.[23–25] Nanoparticle mobility depends on the size of the particles relative to the length scale(s) characterizing the pore size: generally, the quiescent diffusion of particles hindered by geometric confinement slows as the ratio of the

[a] *Chemical and Biomolecular Engineering, University of Houston, Houston, Texas 77204, USA. E-mail: ramanan@uh.edu, jcconrad@uh.edu*
[b] *Chemical and Biomolecular Engineering, University of Melbourne, 3010, Australia*
[c] *Department of Chemistry, University of Houston, Houston, Texas 77204, USA*

† Electronic supplementary information (ESI) available: 6 figures and 3 tables: Fig. S1 (mean-square displacement of nanoparticles in water); Table S1 (models for hindered diffusion); Fig. S2 (probability distribution function of nanoparticle displacements in water); Fig. S3 (decay length for nanoparticles in water); Fig. S4 and associated discussion (calculation of interaction energy for nanoparticles and glass beads); Table S2 (fitting parameters for stretched exponential model); Fig. S5 (complex viscosity of HPAM solution as a function of frequency); Table S3 (sintering protocols for glass beads); Fig. S6 (images and pore size distribution for glass bead packings); Table S4 (total number of trajectories for each bed configuration and fluid); Table S5 (statistics of time points). See DOI: 10.1039/c6sm01543c

particle size to pore size is increased,[26–28] as captured by the ensemble-averaged mean-squared displacement (MSD). Although particles typically exhibit Fickian diffusion on very long time scales even in highly confined porous media, the distributions of their displacements become increasingly non-Gaussian with confinement.[29–31] Fickian but non-Gaussian dynamics arise in a variety of rigid porous media, including polymers in an array of pillars[32] and nanoparticles within a porous matrix of a cured thermoset.[21]

When the fluid through which the particles diffuse is itself complex and contains other species such as proteins, polymers, and/or soft colloids, the fluid constituents (''crowders'') may themselves relax over timescales comparable to that of particle diffusion. Hence the particle dynamics may couple to those of the fluid – while still remaining Fickian diffusive on long time scales. Examples in which this scenario arises include hard sphere colloidal dispersions[15,16] and colloids in a matrix of entangled F-actin polymers.[19] Because these scenarios can also exhibit Fickian but non-Gaussian dynamics, it remains difficult to distinguish the effects of fluid relaxation, related to the dynamics of the medium, from those of geometric confinement. Indeed, this question has motivated a wealth of studies in biophysical settings in which both mobile crowding and immobile confinement affects, *e.g.*, protein conformation and reaction rates.[33–35] Developing insight into the different dynamical signatures arising from complex fluid dynamics and from confinement thus requires systems in which the coupling between dynamics of particles and mobile crowders is well understood.

Towards this end, one particularly simple model of a complex fluid is a solution of unentangled polymers whose radius of gyration is comparable to the size of the diffusing nanoparticles. Particle transport in these systems exhibits striking deviations from the diffusivity predicted from the bulk viscosity.[36–41] A recent scaling analysis predicted that the dynamics of particles in a solution of polymers of comparable size is controlled by the ratio of the particle radius to the polymer correlation length.[42] In a system of polystyrene nanoparticles and semidilute polyelectrolytes, this prediction holds over four orders of magnitude in diffusivity.[43] In addition to dynamical coupling, polymer solutions can also induce attractive depletion interactions between particles or between particles and nearby surfaces that can be described by analytical models.[44–46] Hence particle–polymer fluids are excellent models for controlled studies of dynamics in confined complex fluids.

Here, we identify dynamical signatures arising from spatial confinement from a rigid geometrical structure and from dynamic polymer molecules in the diffusive mobility of nanoparticles. We measure the dynamics of polystyrene nanoparticles of diameter of 400 nm diffusing in packed beds of glass beads of diameter 5.4, 10, or 30 μm. To elucidate the role of non-Newtonian fluid characteristics in dynamics of nanoparticles in complex media, we use three different background matrices: Newtonian water, a Newtonian mixture of glycerol and water, and a non-Newtonian solution of semidilute hydrolyzed polyacrylamide (HPAM). Nanoparticles are imaged using confocal microscopy and tracked over time; from their trajectories, we calculate the distribution of particle displacements and the ensemble-averaged mean-squared displacement. As the confinement length of the packed beds decreases, the dynamics of the nanoparticles become increasingly slow and are well described by hydrodynamic models for hindered diffusion; similarly, the distributions of particle displacements become increasingly non-Gaussian. For nanoparticles diffusing in HPAM, the distribution of particle displacements contains a distinct local maximum centered at zero, indicating an immobile population. By separately analyzing the dynamics of mobile and immobile particles, we show that the diffusivities of mobile nanoparticles approach free diffusion when the dynamics of transiently immobile nanoparticles are excluded. These results are consistent with the idea that the polymer chains mediate dynamical slowing through depletion interactions, which cause particles to transiently adsorb to the bed surfaces. Hence studies of particle dynamics can reveal signatures of the mechanisms by which the interplay of confinement and depletion exacerbates slowing of diffusion of nanoparticles in complex confined media.

Results and discussion

Slowing of diffusive mobility

We use confocal microscopy to investigate the effects of geometrical confinement and solution viscoelasticity on diffusive mobility of 400 nm nanoparticles. To generate geometrical confinement, we fabricate packed beds consisting of glass beads, and report the average pore diameter d_{pore} and the confinement length l_c as a function of bead size (Table 1), as described in the Materials and methods. First, we examine the effects of geometrical confinement on particle mobility in Newtonian solutions. The MSD of nanoparticles in the viscous glycerol/water mixture (G90) is Fickian diffusive at all accessible lag times and decreases as the particles are increasingly confined within the porous beds, as shown in Fig. 1. Even the longest time scales accessible in the experiment are significantly smaller than the average time $t_{diff,0}$ estimated for particles in the center of pores to diffuse to the bead surfaces in the G90 solution, reported in Table 2.

This comparison suggests that a particle located near the center of a pore will not, on average, reach the pore edge. Nonetheless, slowing of the MSD with increasing confinement suggests that the pore geometry affects the diffusive dynamics through hydrodynamic interactions. By contrast, in the same porous medium nanoparticles in water (which is significantly

Table 1 Average porosity, pore size (average chord length), and confinement length (average minimum chord length) of the porous media with bead diameters of 5.4 μm, 10 μm, and 30 μm. The error bar represents the standard deviation of measurements from 25–30 images acquired at different locations within each packed bed

Bead diameter (μm)	Porosity	$d_{pore} = \langle l_{chord} \rangle$ (μm)	$l_c = \langle l_{chord,min} \rangle$ (μm)
5.4	0.36 ± 0.07	4.4 ± 0.8	2.7 ± 0.7
10	0.34 ± 0.06	6.4 ± 1.1	3.7 ± 1.0
30	0.34 ± 0.06	14.7 ± 2.6	8.0 ± 1.1

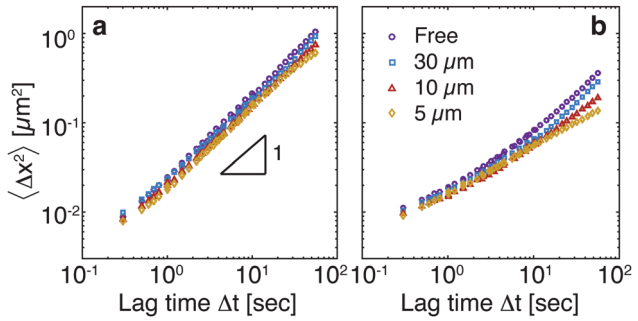

Fig. 1 Mean-squared displacement $\langle \Delta x^2 \rangle$ of 400 nm polystyrene nanoparticles as a function of lag time Δt in (a) glycerol/water mixture (90 w/w%) and (b) HPAM solution (0.1 w/w%). Symbols represent different media: free diffusion in solution (purple circle) or confined diffusion in porous media with bead diameter of 30 μm (blue square), 10 μm (red triangle), or 5 μm (yellow diamond).

less viscous than either solution) exhibit subdiffusive mobility at long time scales or when the particles are highly confined (Fig. S1 in the ESI†). The transition to subdiffusive behavior occurs approximately when particle displacements are comparable to the average confinement length (Table 2). These observations suggest that mobility of nanoparticles in Newtonian solutions that are confined by disordered static obstacles depends on the geometric structure of the pores through hydrodynamic interactions between particles and the surrounding media.

We next examine the dynamics of particles in polymer solutions to identify the effects of crowding on diffusive mobility. In the non-Newtonian semidilute HPAM solution the nanoparticles exhibit subdiffusive dynamics on short time scales, consistent with our previous studies.[41,43] The long-time dynamics, however, depends on the degree of confinement within the bed. As in Newtonian solutions, mobility decreases concomitant with bed particle size (*i.e.* with increasing confinement). The long-time mobility in the least confined bed (d_b = 30 μm) approaches Fickian dynamics as the lag time increases. By contrast, in highly confined beds the dynamics is not completely Fickian even at the longest time scales accessible in these experiments and does not access the long-time diffusive regime. To obtain a lower bound on $t_{diff,0}$ for the HPAM solutions, we instead use the diffusivity of the particles in a bulk unconfined HPAM solution; this choice neglects any changes in diffusivity due to the porous medium itself and provides an upper limit on the diffusivity and a lower limit on $t_{diff,0}$. Again, we find the experimental time scales are shorter than $t_{diff,0}$ (Table 2). These results indicate that in crowded and confined environments, the motion of nanoparticles is highly constrained and is influenced by coupling between dynamics of polymer chains and nanoparticles[43] as well as by the geometric constraints imposed by the stationary bed particles.

Table 2 Estimated time required for particles in the center of a pore to diffuse to the bead surfaces, using the confinement length scale in each packed bed and the long-time diffusion coefficient of unconfined particles in each solution

	$t_{diff,0} = l_c^2/2D_0$ (s)		
Bead diameter (μm)	Water	G90	HPAM
5.4	3	350	1000
10	6	690	2000
30	30	3200	9300

Long-time diffusivity and comparisons to hydrodynamic models

To quantify changes in particle dynamics as a function of geometrical confinement and the solution viscoelasticity, we extract two parameters from the mean-squared displacements. First, from the slope of the long-time MSD we calculate the long time diffusivity D *via* $\langle \Delta x^2(\Delta t) \rangle = 2D\Delta t$, where Δx is the particle displacement at the lag time Δt and the brackets denote time and ensemble averages. Here the long time limit is defined as those time scales that are at least one decade longer than that characterizing the crossover from subdiffusive to diffusive dynamics in the HPAM solution (*i.e.* $>10\tau_c$, where the crossover time $\tau_c \approx 4$ s). We normalize each effective long-time diffusion particle coefficient D by the corresponding free diffusion coefficient in bulk solution D_0 and examine the change in mobility as a function of the dimensionless confinement parameter $\xi = d_{NP}/l_c$. The relative long-time diffusivity D/D_0 decreases with increasing confinement parameter but does not depend strongly on fluid characteristics, as shown in Fig. 2a. Decreases in the long-time diffusivity with increasing confinement were previously measured in structured[19] or unstructured[21,47] porous media. The decrease measured here ($D/D_0 \approx 0.5$–0.65 at $\xi \approx 0.15$) is more pronounced than that measured in earlier experiments in structured porous media, where the diffusivity decreased by only ~10% ($D/D_0 \approx 0.9$) at $\xi \approx 0.15$.[19] By contrast, the relative diffusivity of tracer particles [$D/D_0 \approx \frac{1}{\varphi}\frac{1+2(1-\varphi)-2\varphi\zeta_2}{\varphi-2\varphi\zeta_2}$, ref. 48] was predicted to be slightly faster ($D/D_0 \approx 0.7$) in a random packing of spheres with porosity of $\varphi \approx 0.37$ when hydrodynamic interactions were neglected; ζ_2 is a three-point microstructural parameter that determines the properties of heterogeneous media.[47] These comparisons hint that hydrodynamic and steric interactions mediated by the geometry of random porous media dictate the long-time particle diffusivity even in non-Newtonian solutions.

To account for steric and hydrodynamic effects[49] on diffusivity, several analytical models have been developed to predict the hindrance factor in unstructured porous media consisting of arrays of cylindrical[50,51] or slit[27] pores. The models assume that interactions between particles are negligible, that the background solution can be treated as a dilute continuum, and that the diffusion time is long enough for particles to diffuse throughout the pore cross-section. The models make one of two different assumptions for the estimation of the drag force: (i) in the centerline approximation,[52] the drag force is assumed to be constant over the cross-section and is taken to be the force at the center of the cylinder or slit pore; (ii) in cross-section averaging,[53] the drag force is taken to be a function of the particle distance from the wall. Table S1 (ESI†) summarizes the functional dependence of the analytical models on the dimensionless confinement parameter ($\xi = d_{NP}/l_c$). For $\xi \approx 0.15$–0.05, corresponding

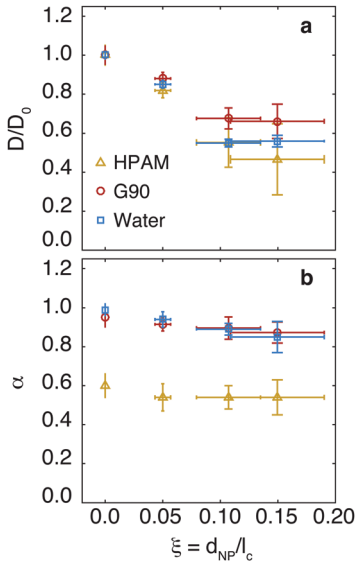

Fig. 2 (a) Normalized effective diffusivity D/D_0 and (b) subdiffusive exponent α as a function of normalized confinement length $\xi = d_{NP}/l_c$ measured for nanoparticles diffusing in different solutions. In (a) the normalized effective diffusivity is extracted from the long time MSD *via* $\langle \Delta x^2 \rangle = 2D\Delta t$. In (b) the subdiffusive exponent is extracted from a power law fit of the MSD *via* $\langle \Delta x^2 \rangle = \beta \Delta t^{\alpha}$ at short times. Symbols represent nanoparticle diffusion in HPAM solution (gold triangle), glycerol/water mixture (red circle), and water (blue square).

to the confinement parameters accessible in our experiments, the relative diffusivities predicted by different models range from $D/D_0 \approx 0.6$–0.8 (Table 3), in reasonable agreement with our results (Table 4). Moreover, these results are consistent with an earlier study of particles diffusing in a disordered polymeric structure with confinement lengths of $\xi \approx 0.02$–0.10 and a porosity of $\varphi \approx 0.52$, in which the relative diffusivities were $D/D_0 \approx 0.4$–0.5.[21] The similarity in the measured and predicted diffusivities thus suggests that hydrodynamic interactions as well as variations in pore arrangement and structure control the long-time diffusive dynamics within disordered porous media, regardless of fluid rheology.

Short-time subdiffusion

Second, from the scaling behavior of the MSD on short time scales we calculate the short time subdiffusive exponent α *via* $\langle \Delta x^2(\Delta t) \rangle = \beta \Delta t^{\alpha}$. The subdiffusive exponent depends only weakly on the confinement parameter in both Newtonian (W, G90) and non-Newtonian (HPAM) solutions, as shown in Fig. 2b. This observation indicates that short time mobility of nanoparticles is not affected by geometric confinement, as the particles on average do not encounter the fixed obstacles at very short times. For Newtonian solutions, α decreases from 1 to 0.9 as confinement is increased. The subdiffusive exponents in HPAM, however, are notably smaller than those measured in Newtonian solutions within the same porous medium and decrease from 0.6 to 0.5. When the dynamics of particles and polymers are fully coupled, the subdiffusive exponent is predicted to be 0.5 from the Rouse dynamics of the polymers;[42] in earlier measurements in the HPAM system the subdiffusive exponent varied between 0.5–1 depending on polymer concentration and particle size, consistent with only partial coupling of the particle dynamics to polymer fluctuations.[43] Hence the short-time subdiffusive behavior of the particles in HPAM solutions is controlled by coupling to the polymer dynamics, in contrast to the hydrodynamically-controlled long-time diffusivity.

Table 4 Normalized diffusivity D/D_0 as a function of confinement parameter for nanoparticle diffusion in glycerol/water (G90), water, and HPAM solution

		D/D_0		
l_c (μm)	ξ	G90	Water	HPAM
2.7	0.15	0.66	0.53	0.47
3.7	0.11	0.68	0.56	0.55
8.0	0.05	0.88	0.85	0.82

Statistics of displacement distributions

To gain further insight into the processes controlling the confined dynamics of nanoparticles in the different solutions, we analyze the distribution of one-dimensional particle displacements $G_s(\Delta x, \Delta t)$ at several lag times and for various solutions and various pore sizes. In free diffusion, the distribution of particle displacements is Gaussian in both Newtonian (Fig. 3a and b) and non-Newtonian HPAM solutions (Fig. 3c and d). As the particles are increasingly confined within the pores, the diffusive mobility of nanoparticles deviates from Gaussian dynamics. In the highly confined bed, the distributions of particle displacements cannot be modeled using a single Gaussian function. Instead, we fit the distributions to the sum of a Gaussian function, to model the center of the distribution, and a stretched exponential function, to model the tail, as[19]

$$G_s(\Delta x, \Delta t) = a_1 \exp\left(-\left(\frac{\Delta x}{\delta}\right)^2\right) + a_2 \exp\left(-\left|\frac{\Delta x}{\gamma(\Delta t)}\right|^s\right), \quad (1)$$

where a_1 and a_2 are pre-exponential factors, δ and $\gamma(\Delta t)$ are the decay lengths for the Gaussian and the stretched exponential models, respectively, and s is the stretching exponent.

Table 3 Normalized diffusivity D/D_0 as a function of confinement parameter, calculated from the models

		Cylindrical pores	Slit pores		
l_c (μm)	ξ	Centerline approximation[54,55]	Cross section averaging[56,57]	Centerline approximation[52]	Cross section averaging[27]
2.7	0.15	0.50	0.48	0.72	0.55
3.7	0.11	0.62	0.58	0.80	0.66
8.0	0.05	0.81	0.76	0.90	0.82

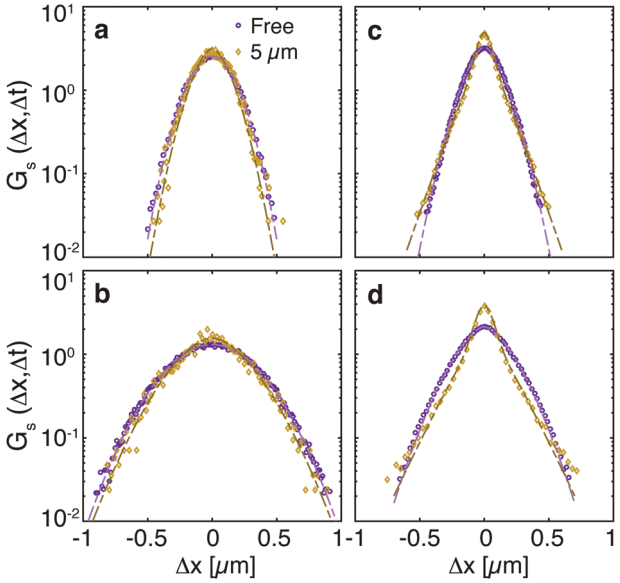

Fig. 3 Probability density function of particle displacements, $G_s(\Delta x, \Delta t)$, at lag times Δt of 1 s (top row) and 5 s (bottom row) for nanoparticles in (a and b) glycerol/water mixture (90 w/w%) and (c and d) HPAM solution (0.1 w/w%). Symbols represent different media: free diffusion in solution (purple circle) and confined diffusion in porous media with bead diameter of 5 μm (yellow diamond). The dashed lines indicate fits to eqn (1).

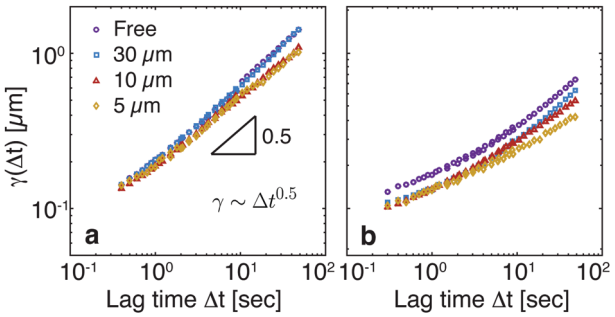

Fig. 4 Decay length as a function of lag time for nanoparticles in (a) glycerol/water mixture (90 w/w%) and (b) HPAM solution (0.1 w/w%). Symbols represent different media: free diffusion in solution (purple circle); confined diffusion in porous media with bead diameter of 30 μm (blue square), 10 μm (red triangle), or 5 μm (yellow diamond).

We hypothesize that the first term describes particles that are nearly immobilized due to trapping or adsorption, and the second term describes particles undergoing untrapped but confined motions. In the initial fitting of the data, we allowed all fitting parameters to float and found that the stretching exponent s and the decay length of the Gaussian model δ were nearly independent of lag time for each solution and bed configuration. We therefore used the average values of $\langle s \rangle$ and $\langle \delta \rangle$ to reduce the number of fitting parameters. For nanoparticles diffusing in Newtonian glycerol/water solutions within confined bed, the pre-exponential fitting factors satisfy $a_1 \ll a_2$, indicating absence of any long-duration trapped states (Fig. 3b). For nanoparticles diffusing in HPAM within the porous media, however, a_1 is not negligible ($a_1/a_2 \approx 0.1$–2), suggesting that a second mechanism affects the diffusion of nanoparticles in the HPAM solution through the porous medium (Fig. 3d).

From the stretched exponential fits we extract the decay length γ, which describes the dynamics of mobile states. For freely-diffusing particles in Newtonian solutions, the decay length increases as the square root of time at all time scales, *i.e.* $\gamma(\Delta t) \sim \sqrt{\Delta t}$ (Fig. 4a). In non-Newtonian solutions, the decay length of freely-diffusing particles on long time scales also grows as the square root of time (Fig. 4b). These distinctive dynamics, previously reported for Fickian but non-Gaussian diffusion in porous media,[19] in hard sphere colloidal suspensions,[31] and in entangled F-actin networks,[29] were proposed to generically arise in heterogeneous media.[29–31] In this picture, slow relaxations of the media or local deviations in confining geometry resulted in temporal and/or spatial variations in the local environment. These variations generated a distribution of local particle diffusivities, leading to a non-Gaussian distribution of particle displacements. By contrast, the decay length of strongly-confined particles grows more slowly with lag time than the predicted square-root dependence[29–31] for both glycerol/water and HPAM solutions. Hence in strong confinement diffusive dynamics depends on both pore structure and time scale, regardless of the presence of polymer crowders. As one extreme example, the local diffusive dynamics of particles in water (Fig. S1–S3 in the ESI†) changes as the pore size and diffusion length scale become comparable and is non-Fickian even in weak confinement.

Particle trajectories reveal transient adsorption

Next, to understand the origin of the caged or trapped motion we examine the trajectories of particles diffusing freely and confined by porous media and/or polymers in solution. In Newtonian glycerol/water solutions, particle trajectories show random diffusion. Particles undergo larger displacements over successive time steps (Δt = 0.5 s) when freely diffusing than when diffusing in a highly confined porous medium (Fig. 5a and b). Particles in the glycerol/water solution within the porous medium are slightly hindered by geometric confinement but nonetheless remain mobile throughout (Fig. 5b). This result is consistent with earlier measurements of confined diffusion near walls[18,58] and in pores.[25,59,60] Conversely, the trajectories of unconfined and of confined nanoparticles diffusing in HPAM solutions exhibit qualitatively different features (Fig. 5c and d). Unconfined nanoparticles in HPAM exhibit diffusive trajectories, and the displacements over time do not exhibit long waiting times or jumps between frames. When highly confined by a porous medium, however, the trajectories of nanoparticles in HPAM reveal long intervals of near-zero displacements that are separated by random motions. Here the lengthy dwell time between random motions likely arises due to temporary adsorption of the particles onto the surface of the glass beads (Fig. 5d).

Similar trajectories featuring long-duration immobilizations interrupted by intermittent jumps were observed for polymer chains diffusing near a surface.[32,61,62] Polymer chains in these experiments could loosely bind to the surface but frequently

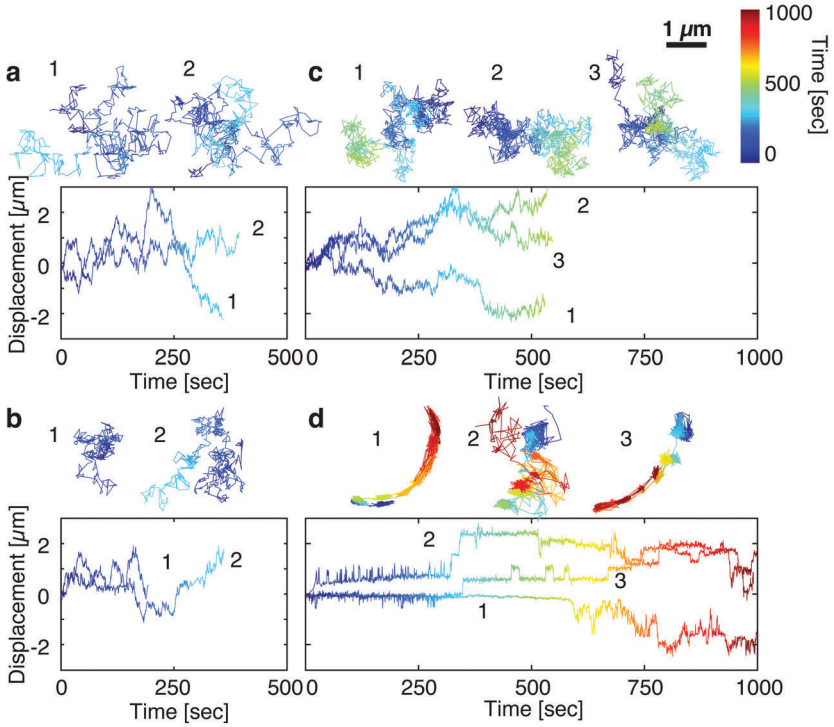

Fig. 5 Representative trajectories and corresponding displacements as a function of time for nanoparticles diffusing in (a and b) glycerol/water mixture (90 w/w%) and (c and d) HPAM solution (0.1 w/w%). The top row [(a and c)] shows free diffusion in solution and the bottom row [(b and d)] shows confined diffusion in porous media with a bead diameter of 5 μm.

desorbed, as indicated by a rapid jump in position. After desorbing, chains could either diffuse back to the bulk or re-adsorb onto the surface (either permanently or transiently). We posit that the tendency for particles in HPAM to become temporarily immobilized when diffusing in porous media is mediated by the presence of the polymer molecules. This idea is consistent with the increasingly pronounced local maximum at zero in the distribution of particle displacements at longer lag times. Moreover, the total interaction potential (the sum of electrostatic, van der Waals, and depletion[45] interactions) exhibits a weak minimum of depth $\sim 5\ kT$ (Fig. S4 in the ESI†) consistent with transient adsorption. Hence these experiments reveal that the local mobility of nanoparticles in non-Newtonian solutions is significantly affected both by macromolecule-mediated depletion interactions and by confinement.

Distributions of mobile and immobile times

To separate effects of confinement on particle dynamics from those induced by the polymers, we first define an absolute displacement of $r = 0.045$ μm as the threshold of particle immobility; this value corresponds to the resolution of the tracking algorithm under these imaging conditions. Using this immobility threshold, we binarize the particle displacements over consecutive time steps: displacements greater than this threshold are labeled "1" and those less than this threshold are labeled "0". This process converts trajectories into strings of ones and zeroes. We then calculate the distribution of the immobile (consecutive zeros, τ_{im}) and mobile (consecutive ones, τ_{mob}) steps for each trajectory. For nanoparticles in glycerol/water the ensemble-aggregated distributions of mobile and of immobile steps both follow an exponential decay, independent of the confinement imposed by the porous structure (Fig. 6a and b). The distribution of mobile steps in non-Newtonian HPAM also follows an exponential decay, independent of confinement (Fig. 6c); similarly, the distribution of immobile times in unconfined non-Newtonian HPAM is also exponential (Fig. 6d).

The distribution of immobile times, however, deviates from an exponential decay when the nanoparticles are confined within a porous medium. We therefore test alternate fitting functions to model these distributions. A power-law function[63] of exponent ~ 3, which would suggest a spectrum of binding energies, can adequately describe the long-time portion of the distribution, but cannot capture the short-time limit. Instead, we fit this distribution to a stretched exponential decay with a stretching exponent of $\beta = 0.63$–0.66 (Fig. 6d and Table S2 in the ESI†). This stretching exponent is close to that predicted for the survival time distribution in a universalist diffusion-within-traps model in three dimensions ($d = 3$), $\beta = d/d + 2 = 0.6$ [ref. 64], suggesting that the asymmetry in the immobile *versus* mobile time distribution arises from particle adsorption onto the bed surface. In diffusion-with-traps models, particles diffuse to local sinks or traps and become immobilized there. The key assumption underlying these models is that the relaxation time distribution depends both on the time to diffuse to trap sites and on the time for particles to adsorb there.[64] Adsorption of the particles onto the bed and/or

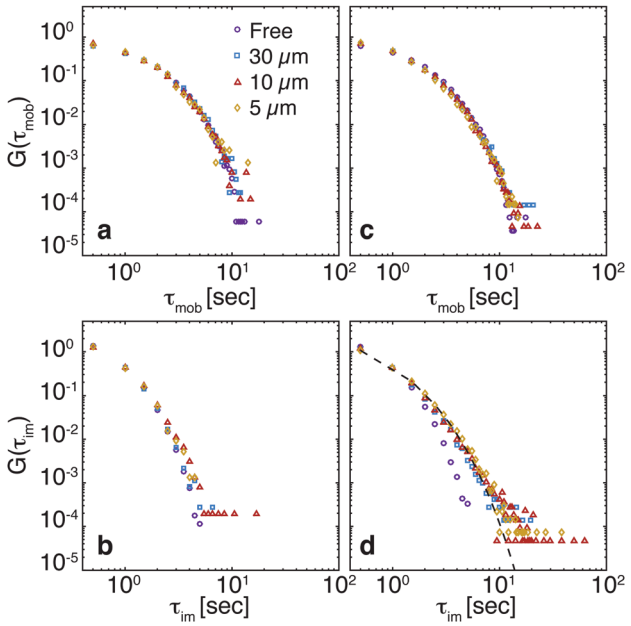

Fig. 6 Probability density function of mobile (top row, [(a and c)]) and immobile (bottom row, [(b and d)]) times for nanoparticles in (a and b) glycerol/water mixture (90 w/w%) and (c and d) HPAM solution (0.1 w/w%). Symbols represent different media: free diffusion in solution (purple circle), confined diffusion in porous media with bead diameter of 30 μm (blue square), 10 μm (red triangle), and 5 μm (yellow diamond). The dashed line in (d) indicates a fit to a stretched exponential function with exponent 0.6.

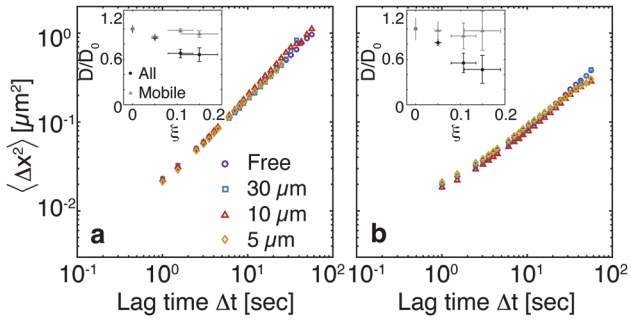

Fig. 7 Mean square displacement of mobile particles as a function of lag time in (a) glycerol/water mixture (90 w/w%) and (b) HPAM solution (0.1 w/w%). Mobile particles are defined as those with displacements larger than the minimum displacement (r = 0.045 μm) resolvable using the tracking algorithm. Symbols represent different media: free diffusion in solution (purple circle), confined diffusion in porous media with bead diameter of 30 μm (blue square), 10 μm (red triangle), and 5 μm (yellow diamond). Inset in each panel: long time diffusion coefficient as a function of confinement parameter for all time step (black circle) and mobile time steps (gray triangle). The long-time diffusivity in confined media approaches that in free solution when the immobile time steps are removed.

exclusion of finite-size particles from small pores[21,65] could generate the effective local traps; we note that HPAM does not irreversibly adsorb to the particle surfaces,[41] ruling out polymer-induced drag. The stretched exponential dynamics appear only when polymer crowders interact with the porous media, and hence are consistent with coupling of polymer-mediated depletion interactions[44–46] with hydrodynamic screening to generate trap sites for particles on the bed surface.

To distinguish the effects of hydrodynamic screening (*cf.* Table 4) from those due to temporary adsorption (*cf.* Fig. 6), we eliminate immobile steps from particle trajectories; here immobile steps are defined as those of duration greater than three consecutive time steps (1.5 s). When the immobile steps are removed, the MSD of mobile particles in confined media approaches that of free diffusion in both Newtonian and non-Newtonian solutions (Fig. 7). Furthermore, the relative diffusion coefficient (D/D_0) extracted from the long-time Fickian diffusion is nearly independent of the confinement parameter (Fig. 7, inset). The MSD of mobile particles in glycerol/water solution is almost identical for the different porous media, consistent with the idea that hydrodynamic interactions with nearby surfaces generate the slowing of diffusion in Newtonian glycerol/water. When the hydrodynamic interactions are removed, mobility is fully recovered. By contrast, in HPAM solution the diffusion of mobile particles at the smallest porous bed (d_b = 5 μm) is very slightly faster than free diffusion on the shortest time scales. This finding is consistent with the anomalously large tails in the distribution of particle displacements in strong confinement (Fig. 3c and d). Local inhomogeneities in the HPAM concentration, whether due to adsorption of polymer molecules onto the surface of glass beads or to hindered transport of the high-molecular-weight polymer into highly confined pores, and/or volume exclusion of the particles from inaccessible small pores may generate the larger-than-expected displacements in the tails of the displacement distributions and hence the faster-than-expected local diffusion of the particles.

Conclusions

We separate the effects of disordered spatial confinement and polymer crowding, using well-characterized polymer solutions and packed beds, on diffusive mobility of nanoparticles. Diffusive mobility decreases as particles in both Newtonian and non-Newtonian solutions are increasingly confined. In both Newtonian and non-Newtonian solutions, hydrodynamic interactions give rise to slowing of diffusive mobility with increasing confinement by the packed beds. Particles diffusing in non-Newtonian fluids, however, exhibit subdiffusive behavior reflecting coupling to the polymer dynamics. The disordered and heterogeneous geometrical structure of the porous media leads to greater decreases in particle diffusivity compared to that measured in ordered structures with comparable pore size. In the non-Newtonian solution an additional mechanism, immobilization of particles on the bed surface, also leads to slowing of diffusion; this immobilization arises from temporary adsorption of the particles onto the surface of glass beads. This feature suggests that presence of long-chain polymer molecules also alters the pore scale mobility of the particles through depletion interactions. Mobility of nanoparticles in HPAM solution through porous media is therefore not only controlled by hydrodynamic interactions, but also by depletion interactions

that generate an adsorption–desorption process. Our analyses thus allow sensitive tests of different mechanisms that slow diffusion, and highlight distinct signatures arising from polymer viscoelasticity – subdiffusion – and crowding – transient immobilization – as opposed to rigid confinement, which controls the slowing of long-time diffusion.

As one example, we suggest that the striking change in the distribution of immobile times upon addition of polymer crowders arises from depletion-mediated adsorption of particles on the bed surface. In a packed bed imbibed with a Newtonian fluid, the exponential distribution of immobile times is consistent with a single characteristic energy for adsorption (or desorption). The unanticipated appearance of a stretched exponential distribution in a confined and crowded system, however, suggests a more complex origin of the dynamics. We propose that particles adsorb transiently to the bed, and hence model the waiting time distribution using a 3-d diffusion-to-traps model[64] in which particles adsorb at local sinks within the medium. Trap models assume irreversible adsorption (an infinite attraction), whereas our depletion attraction is finite. Although the stretching exponent is insensitive to attraction strength, we expect that changes in the characteristic time scale could be used to probe strong polymer-mediated depletion interactions in complex confined media. Likewise, deviations from stretched-exponent dynamics could signal changes in the controlling physical mechanism by which polymers alter the particle dynamics. Hence we expect that sensitive measurements of the statistics of particle dynamics in complex fluids and near surfaces can be used to identify mechanisms controlling nanoparticle transport.

Materials and methods

Preparation of nanoparticle dispersions in Newtonian and non-Newtonian solutions

Fluoro-Max dyed red aqueous fluorescent polystyrene nanoparticles of diameter d_{NP} = 400 nm at concentration of 1 wt% (coefficient of variation of $<5\%$) were purchased from Thermo Fisher Scientific. Hydrolyzed polyacrylamide (HPAM) polymer of weight-averaged molecular weight (M_w) of 8 000 000 Da (FLOPAAM 3330) was provided by SNF. The degree of hydrolysis was 25–30%, as reported by the manufacturer. We prepared an aqueous solution of HPAM in deionized water with concentration of c_{HPAM} = 0.1 wt%, corresponding to a normalized polymer concentration of c/c^* = 6.5 in the semidilute regime. The radius of gyration and the correlation length were estimated from scaling relationships as 205 nm and 72 nm, respectively.[43] The rheological properties of the HPAM solution were measured using an ARES rheometer from Rheometric Scientific equipped with Couette geometry (inner diameter of 32 mm and outer diameter of 34 mm). Specifically, we measured the elastic ($G'(\omega)$) and loss ($G''(\omega)$) moduli of the HPAM solution as a function of frequency (ω = 0.01–100 rad s^{-1}) in the linear viscoelastic regime, and calculated the complex viscosity as $\eta^*(\omega) = [G'^2(\omega) + G''^2(\omega)]^{1/2}/\omega$ (Fig. S5 in the ESI†). We also prepared a glycerol/water mixture at a concentration of 90 wt% of glycerol (G90) in which to measure particle dynamics at a comparable value of the local viscosity and so isolate the effects of the polymer dynamics. Polystyrene nanoparticles were added to the HPAM solution, the G90 solution, and the deionized water at a concentration of 2×10^{-3} wt%. The nanoparticle-solution dispersions were then tumbled on a roll mill for 6–24 h to ensure that particles and solutions were uniformly dispersed.

Fabrication of porous media

We purchased borosilicate capillary cells of square cross section with inner side length of 0.7 mm, wall thickness of 0.14 mm, and length of 5 cm from VitroCom, and borosilicate glass microspheres with diameter of 5.4 ± 0.3 μm and 10.0 ± 1.0 μm and soda lime glass microspheres with diameter of 30.1 ± 1.1 μm from Thermo-Scientific. To fabricate 3D porous media, square capillaries were filled with mono-dispersed glass particles to a length of 5 mm. We then lightly sintered (Table S3 in the ESI†) the glass particles to permanently fix them in the square channel.

Characterization of pore and throat size of porous media

We visualized the bed structure by imbibing each bed with a solution of rhodamine-B (Wako Pure Chemical Industries, Ltd) in a mixture of carbon disulfide (n = 1.63) and ethanol (n = 1.36). The amount of each mixture component was selected to match the refractive index of soda lime (n = 1.52) or borosilicate (n = 1.56) glass beads. Confocal micrographs of beds with bead diameters of 5.4 μm, 10 μm, and 30 μm reveal a connected pore network (Fig. S6a–c, ESI†). We acquired 25–30 2-d images at different locations in the beds and subsequently binarized them to identify pores and bed particles.

To characterize the bed structure we measured two characteristic length scales, the pore size and confinement length, from the binarized confocal micrographs of the beds. First, 5000 points were randomly selected inside the pore space in each binarized image. At each point, eight vectors that were equally spaced in the angular direction were expanded in both negative and positive directions until they met the edges of the glass beads. For each point and direction, the chord length was calculated as the sum values of negative and positive vectors. We defined the minimum chord length as the minimum value of chord lengths at each point among all the angular directions.[66] The probability distribution functions (PDFs) of the chord length and the minimum chord length in porous media, shown in Fig. S6d–f (ESI†) for bead diameters of 5.4 μm, 10 μm, and 30 μm, are best fit to a gamma function,

$$G(l_{chord}) = \frac{1}{b^a \Gamma(a)} l_{chord}^{a-1} \exp\left(-\frac{l_{chord}}{b}\right), \quad (2)$$

where l_{chord} is the chord length, $G(l_{chord})$ is the probability distribution of the chord length, and a and b are fitting parameters. Finally, we defined the pore size as the average chord length and the confinement length as the average minimum chord length. Table 1 contains the average porosity, pore size, and confinement length of each porous medium as a function of the bead diameter. The average bed porosity $\varphi \approx 35\%$ is roughly

constant across the different porous beds studied. The average pore size d_{pore} varies between 4.4 ± 0.8 and 14.7 ± 2.6 μm and the confinement length l_c varies between 2.7 ± 0.7 and 8.0 ± 1.1 μm. We defined a dimensionless confinement length $\xi = d_{NP}/l_c$ as the ratio of the particle diameter to the pore size.

Imaging of nanoparticles diffusing through porous media

We imaged the nanoparticles as they diffused in the different fluids using a SP8 Leica inverted confocal microscope equipped with a 40× immersion oil lens of numerical aperture (NA) 1.30. Particles were imaged at a distance of z = 18–20 μm above the capillary wall in porous beds with bead diameter of d_b = 30 μm and at z = 7–8 μm above the capillary wall for beds with bead diameters of d_b = 5 μm and 10 μm. We acquired movies at 2 and 10 frames per second (fps) for nanoparticles diffusing in HPAM and glycerol/water and at 10 and 40 fps for nanoparticles diffusing in water. The image pixel size was 0.284 μm per pix and the image size was 145.3 × 145.3 μm^2. We acquired twenty movies of each sample at different locations to increase the total number of observed particles, which varied between 100–1000.

Tracking of nanoparticles in porous media

A single-particle tracking algorithm[67] was applied to locate and track the nanoparticles over time with spatial resolution of ε = 45 nm. From the particle trajectories, we calculated the time-dependent displacement and the ensemble-averaged mean-squared displacement (MSD) of the particles. MSDs are reported only for values exceeding $2\varepsilon^2$, which corresponded to the minimum displacement resolvable by the tracking algorithm. Particles that were aggregated or whose maximum displacement was less than 2 pixels (0.56 μm, comparable to their diameter) over the duration of the experiment were excluded from the data analysis. The total number of trajectories for each fluid/bed combination and frame rate is given in Table S4 (ESI†); the number of time points analyzed for each fluid/bed combination and frame rate at short and at long times is given in Table S5 (ESI†).

Acknowledgements

R. K. acknowledges funding from ExxonMobil Company. J. C. C. acknowledges funding from NSF (CBET-1438204) and the Welch Foundation (E-1869). We thank J. C. Palmer for assistance with the interaction potential calculations and for helpful feedback on the manuscript.

References

1 M. C. Konopka, I. A. Shkel, S. Cayley, M. T. Record and J. C. Weisshaar, *J. Bacteriol.*, 2006, **188**, 6115–6123.
2 C. E. J. Dieteren, S. C. A. M. Gielen, L. G. J. Nijtmans, J. A. M. Smeitink, H. G. Swarts, R. Brock, P. H. G. M. Willems and W. J. H. Koopman, *Proc. Natl. Acad. Sci. U. S. A.*, 2011, **108**, 8657–8662.
3 F. Roosen-Runge, M. Hennig, J. Zhang, R. M. J. Jacobs, M. Sztucki, H. Schober, T. Seydel and F. Schreiber, *Proc. Natl. Acad. Sci. U. S. A.*, 2011, **108**, 11815–11820.
4 F. Höfling and T. Franosch, *Rep. Prog. Phys.*, 2013, **76**, 046602.
5 S. M. A. Tabei, S. Burov, H. Y. Kim, A. Kuznetsov, T. Huynh, J. Jureller, L. H. Philipson, A. R. Dinner and N. F. Scherer, *Proc. Natl. Acad. Sci. U. S. A.*, 2013, **110**, 4911–4916.
6 R. Tang, C. S. Kim, D. J. Solfiell, S. Rana, R. Mout, E. M. Velázquez-Delgado, A. Chompoosor, Y. Jeong, B. Yan, Z.-J. Zhu, C. Kim, J. A. Hardy and V. M. Rotello, *ACS Nano*, 2013, **7**, 6667–6673.
7 E. Vlashi, L. E. Kelderhouse, J. E. Sturgis and P. S. Low, *ACS Nano*, 2013, **7**, 8573–8582.
8 A. Parodi, S. G. Haddix, N. Taghipour, S. Scaria, F. Taraballi, A. Cevenini, I. K. Yazdi, C. Corbo, R. Palomba, S. Z. Khaled, J. O. Martinez, B. S. Brown, L. Isenhart and E. Tasciotti, *ACS Nano*, 2014, **8**, 9874–9883.
9 G. Z. Jin, M. Eltohamy and H. W. Kim, *RSC Adv.*, 2015, **5**, 26832–26842.
10 M. Bramini, D. Ye, A. Hallerbach, M. Nic Raghnaill, A. Salvati, C. Åberg and K. A. Dawson, *ACS Nano*, 2014, **8**, 4304–4312.
11 V. Rebbin, R. Schmidt and M. Fröba, *Angew. Chem., Int. Ed.*, 2006, **45**, 5210–5214.
12 D. S. Novikov, E. Fieremans, J. H. Jensen and J. A. Helpern, *Nat. Phys.*, 2011, **7**, 508–514.
13 K. I. Winey and R. A. Vaia, *MRS Bull.*, 2007, **32**, 314–319.
14 S. K. Kumar and R. Krishnamoorti, *Annu. Rev. Chem. Biomol. Eng.*, 2010, **1**, 37–58.
15 S. Gam, J. S. Meth, S. G. Zane, C. Chi, B. A. Wood, K. I. Winey, N. Clarke and R. J. Composto, *Soft Matter*, 2012, **8**, 6512–6520.
16 R. Li, J. A. Fowler and B. A. Todd, *Phys. Rev. Lett.*, 2014, **113**, 028303.
17 R. Raccis, A. Nikoubashman, M. Retsch, U. Jonas, K. Koynov, H.-J. Butt, C. N. Likos and G. Fytas, *ACS Nano*, 2011, **5**, 4607–4616.
18 P. K. Ghosh, P. Hänggi, F. Marchesoni, S. Martens, F. Nori, L. Schimansky-Geier and G. Schmid, *Phys. Rev. E: Stat., Nonlinear, Soft Matter Phys.*, 2012, **85**, 011101.
19 K. He, F. Babaye Khorasani, S. T. Retterer, D. K. Thomas, J. C. Conrad and R. Krishnamoorti, *ACS Nano*, 2013, **7**, 5122–5130.
20 F. D. A. Aarão Reis and D. Di Caprio, *Phys. Rev. E: Stat., Nonlinear, Soft Matter Phys.*, 2014, **89**, 062126.
21 M. J. Skaug, L. Wang, Y. Ding and D. K. Schwartz, *ACS Nano*, 2015, **9**, 2148–2156.
22 M. J. Skaug and D. K. Schwartz, *Ind. Eng. Chem. Res.*, 2015, **54**, 4414–4419.
23 J. Kirstein, B. Platschek, C. Jung, R. Brown, T. Bein and C. Bräuchle, *Nat. Mater.*, 2007, **6**, 303–310.
24 P. Hänggi and F. Marchesoni, *Rev. Mod. Phys.*, 2009, **81**, 387–442.
25 P. S. Burada, P. Hänggi, F. Marchesoni, G. Schmid and P. Talkner, *ChemPhysChem*, 2009, **10**, 45–54.
26 H. Brenner and L. J. Gaydos, *J. Colloid Interface Sci.*, 1977, **58**, 312–356.

27 Y. Pawar and J. L. Anderson, *Ind. Eng. Chem. Res.*, 1993, **32**, 743–746.
28 J. D. C. Jacob, K. He, S. T. Retterer, R. Krishnamoorti and J. C. Conrad, *Soft Matter*, 2015, **11**, 7515–7524.
29 B. Wang, S. M. Anthony, S. C. Bae and S. Granick, *Proc. Natl. Acad. Sci. U. S. A.*, 2009, **106**, 15160–15164.
30 B. Wang, J. Kuo, S. C. Bae and S. Granick, *Nat. Mater.*, 2012, **11**, 481–485.
31 J. Guan, B. Wang and S. Granick, *ACS Nano*, 2014, **8**, 3331–3336.
32 D. Wang, C. He, M. P. Stoykovich and D. K. Schwartz, *ACS Nano*, 2015, **9**, 1656–1664.
33 H.-X. Zhou, G. Rivas and A. P. Minton, *Annu. Rev. Biophys.*, 2008, **37**, 375–397.
34 A. Malik, J. Kundu, S. K. Mukherjee and P. K. Chowdhury, *J. Phys. Chem. B*, 2012, **116**, 12895–12904.
35 M. R. Hilaire, R. M. Abaskharon and F. Gai, *J. Phys. Chem. Lett.*, 2015, **6**, 2546–2553.
36 M. Mackay, T. T. Dao, A. Tuteja, D. L. Ho, B. van Horn, H. Kim and C. J. Hawker, *Nat. Mater.*, 2003, **2**, 762–766.
37 A. Tuteja, M. E. Mackay, S. Narayanan, S. Asokan and M. S. Wong, *Nano Lett.*, 2007, **7**, 1276–1281.
38 R. A. Omari, A. M. Aneese, C. A. Grabowski and A. Mukhopadhyay, *J. Phys. Chem. B*, 2009, **113**, 8449–8452.
39 N. Ziebacz, S. A. Wieczorek, T. Kalwarczyk, M. Fialkowski and R. Holyst, *Soft Matter*, 2011, **7**, 7181–7186.
40 I. Kohli and A. Mukhopadhyay, *Macromolecules*, 2012, **45**, 6143–6149.
41 F. Babaye Khorasani, R. Poling-Skutvik, R. Krishnamoorti and J. C. Conrad, *Macromolecules*, 2014, **47**, 5328–5333.
42 L.-h. Cai, S. Panyukov and M. Rubinstein, *Macromolecules*, 2011, **44**, 7853–7863.
43 R. Poling-Skutvik, R. Krishnamoorti and J. C. Conrad, *ACS Macro Lett.*, 2015, **4**, 1169–1173.
44 D. Rudhardt, C. Bechinger and P. Leiderer, *Phys. Rev. Lett.*, 1998, **81**, 1330–1333.
45 R. Tuinier, D. G. A. L. Aarts, H. H. Wensink and H. N. W. Lekkerkerker, *Phys. Chem. Chem. Phys.*, 2003, **5**, 3707–3715.
46 D. Kleshchanok, R. Tuinier and P. R. Lang, *J. Phys.: Condens. Matter*, 2008, **20**, 073101.
47 H. Liasneuski, D. Hlushkou, S. Khirevich, A. Höltzel, U. Tallarek and S. Torquato, *J. Appl. Phys.*, 2014, **116**, 034904.
48 S. Torquato, *J. Appl. Phys.*, 1985, **58**, 3790–3797.
49 P. Dechadilok and W. M. Deen, *Ind. Eng. Chem. Res.*, 2006, **45**, 6953–6959.
50 M. G. Davidson and W. M. Deen, *Macromolecules*, 1988, **21**, 3474–3481.
51 S. G. J. M. Kluijtmans, J. K. G. Dhont and A. P. Philipse, *Langmuir*, 1997, **13**, 4982–4987.
52 J. Happel and H. Brenner, *Low reynolds number hydrodynamics: with special applications to particulate media*, Springer Science & Business Media, 2012.
53 P. Ganatos, R. Pfeffer and S. Weinbaum, *J. Fluid Mech.*, 1980, **99**, 755–783.
54 J. R. Pappenheimer, E. M. Renkin and L. M. Borrero, *Am. J. Physiol.*, 1951, **167**, 13–46.
55 E. M. Renkin, *J. Gen. Physiol.*, 1954, **38**, 225–243.
56 G. M. Mavrovouniotis and H. Brenner, *J. Colloid Interface Sci.*, 1988, **124**, 269–283.
57 J. J. L. Higdon and G. P. Muldowney, *J. Fluid Mech.*, 1995, **298**, 193–210.
58 M. A. Bevan and D. C. Prieve, *J. Chem. Phys.*, 2000, **113**, 1228–1236.
59 A. Imperio, J. T. Padding and W. J. Briels, *J. Chem. Phys.*, 2011, **134**, 154904.
60 S. L. Eichmann, B. Smith, G. Meric, D. H. Fairbrother and M. A. Bevan, *ACS Nano*, 2011, **5**, 5909–5919.
61 C. Yu, J. Guan, K. Chen, S. C. Bae and S. Granick, *ACS Nano*, 2013, **7**, 9735–9742.
62 M. J. Skaug, J. Mabry and D. K. Schwartz, *Phys. Rev. Lett.*, 2013, **110**, 256101.
63 M. J. Skaug, J. N. Mabry and D. K. Schwartz, *J. Am. Chem. Soc.*, 2014, **136**, 1327–1332.
64 J. C. Phillips, *Rep. Prog. Phys.*, 1996, **59**, 1133–1207.
65 A.-Y. Jee, J. L. Curtis-Fisk and S. Granick, *Macromolecules*, 2014, **47**, 5793–5797.
66 D. Stoeckel, C. Kübel, K. Hormann, A. Höltzel, B. M. Smarsly and U. Tallarek, *Langmuir*, 2014, **30**, 9022–9027.
67 J. C. Crocker and D. G. Grier, *J. Colloid Interface Sci.*, 1996, **179**, 298–310.

